# A generalised approach on kerf geometry prediction during $CO_2$ laser cut of PMMA thin plates using neural networks

**John Dimitrios Kechagias** ( jkechag@teilar.gr )
University of Thessaly https://orcid.org/0000-0002-5768-4285
**Konstantinos Ninikas**
University of Thessaly
**Panagiotis Stavropoulos**
University of Patras
**Konstantinos Salonitis**
Cranfield University

**Research Article**

**Keywords:** Neural Networks, FFBP, Laser Cutting, modelling, Kerf

**Posted Date:** September 3rd, 2021

**DOI:** https://doi.org/10.21203/rs.3.rs-268745/v2

## Abstract

This study presents an application of feedforward and backpropagation neural network (FFBP-NN) for predicting the kerf characteristics, i.e. the kerf width in three different distances from the surface (upper, middle and down) and kerf angle during laser cutting of 4 mm PMMA (polymethyl methacrylate) thin plates. Stand-off distance (SoD: 7, 8 and 9 mm), cutting speed (CS: 8, 13 and 18 mm/sec) and laser power (LP: 82.5, 90 and 97.5 W) are the studied parameters for low power $CO_2$ laser cutting. A three-parameter three-level full factorial array has been used, and twenty-seven ($3^3$) cuts are performed. Subsequently, the upper, middle and down kerf widths (Wu, Wm and Wd) and the kerf angle (KA) were measured and analysed through ANOM (analysis of means), ANOVA (analysis of variances) and interaction plots. The statistical analysis highlighted that linear modelling is insufficient for the precise prediction of kerf characteristics. An FFBP-NN was developed, trained, validated and generalised for the accurate prediction of the kerf geometry. The FFBP-NN achieved an R-all value of 0.98, in contrast to the ANOVA linear models, which achieved Rsq values of about 0.86. According to the ANOM plots, the parameter values which optimize the KA resulting in positive values close to zero degrees were the 7 mm SoD, 8 mm/s CS and 97.5 W LP.

## Article Highlights

- Application of FFBP-NN to predict kerf geometry during laser cutting of PMMA thin plates
- Robust design using full orthogonal experimental arrays
- Accurate predictions of kerf widths and kerf angle
- Map min-max method is adopted for data normalization

## 1. Introduction

Any material removal process utilising a laser beam as a cutting tool presents many benefits such as fast cutting speed (and thus higher productivity rates), high accuracy, good control of the Heat Affected Zone (HAZ) and minimal deformation, especially when low power $CO_2$ lasers are used [1,2]. Low power lasers are employed to process polymer-based materials in a wide range of applications [3-6]. The material melts and evaporates quickly during the laser cutting process, mainly due to the favourable material thermal properties and the beam density [7-9]. Laser processing of the PMMA thermoplastic is used in various applications like automotive and transportation (bumpers, panels, fenders), electronics (screens made from PMMA, covers for PC or 3D printers, etc.), furniture (door canopies, functional balustrades), welfare (cabinets), lighting (transparency and brilliance optical applications), etc. [10-15].

The cutting quality is characterised through a number of features, such as the kerf width, the kerf angle, the roughness of the edge, the formation of burrs, and the depth of the HAZ to name few [1]. For assessing the state of the art, a thorough literature review was undertaken. A number of academic libraries and databases were queried using relevant search strings, such as “laser” AND “cut” AND “PMMA”. Scopus indicated that over the last 20 years more than one hundred papers have been presented on this topic. However, very few researches have been focused on PMMA kerf width and kerf angle optimisation and modeling (nine was found using “laser” AND “cut” AND “PMMA” AND “kerf”). In the following paragraphs, the more relevant and significant studies are being reviewed and discussed.

Kerf width is one of the most studied factors for the laser cutting quality performance [16-18] of thin thermoplastic materials and is affected by a number of process parameters such as the focusing distance, spot diameter, cutting speed, assist-gas pressure and laser power (see Fig.1; [2,7]).

A wide experimental range of laser power and cutting speed values has been investigated in the literature [19-21]. The kerf characteristics (upper and bottom width, melted transverse area, melted volume per unit time and mean roughness values on cut edges) were measured by Caiazzo et al. [21]. The laser power (200-1400 W) and the cutting speed (18-150 mm/s) are optimised for the $CO_2$ laser cutting of polymeric materials (PE, PC, PP) of different thicknesses (2 - 10 mm) using the ‘trial and error’ experimental method. The focal length was 127 mm, and the focal spot diameter adjusted to 0.2-0.3 mm. Such process parameters resulted in kerf widths (upper and bottom) between 0.1 to 0.5 mm and average roughness (Ra) of up to 5 μm. The researchers, however, did not propose any model for predicting the process performance. They concluded that lower power values are suitable for cutting polymeric materials and that the laser cutting speed is a critical parameter.

A preliminary evaluation of the results of the cutting parameters in a range of polymeric materials (PMMA, PC, PP, etc.) was carried out by Davim et al. [1]. They studied the quality of cut (burr length and heat-affected zone depth) without trying to model the quality metrics. Thin (6 mm) PMMA plates were cut using $CO_2$ laser (high frequency, continuous mode, Gaussian profile) with power in the range between 350 and 650 Watt and cutting speed between 25 to 58 mm/s [19]. The focal spot size was about 0.3 mm, and the focal depth about 1.5 mm. Surface roughness parameters (Ra, Rt, Rz, Rp), dimensional precision and the depth of the heat-affected zone were studied and optimised using evolution diagrams of each metric according to the cutting speed and laser power. They have measured the depth of the HAZ between 0.12 to 0.37 mm, without burr and low average surface roughness (Ra < 1 μm). It concluded that when the laser power increases, the depth of the HAZ also increases and the roughness decreases. In contrast, the opposite effects are being observed when the cutting speed increases. No mathematical model (analytical or experimental) was developed for the above-studied kerf characteristics.

The effects of laser power (0.275 - 2.5 W) and cutting speed (7 – 64 mm/s) of $CO_2$ laser on the width and depth of micro-channels manufactured from (1 mm) PMMA of different molecular weights have been investigated experimentally by Nayak et al. [20]. The laser had a wavelength of 10.6 μm, lens focal length of 50.8 mm, spot size up to 0.13mm and a maximum power of 25 W. They found that the depth increases with an increase in power or a decrease in beam speed, or a decrease in molecular weight. The width increases with a laser power surge. As with the previous studies, no predictive models for depth and width were proposed.

The impact of the spot diameter (focal length 200-210 mm), laser beam speed and incident power during PMMA miniaturised structures processed by a low power $CO_2$ laser (50 W, Gaussian continuous wave, minimum spot radius about 0.25 mm) have been investigated experimentally by Romoli et al. [3]. By incorporating an analytical model for the depth of cut and an empirical model for the width, the laser power and speed optimized, achieving depths between 0.05 and 0.6 mm as well as various widths from 0.15 to 0.4 mm

Varsi and Shaikh [18] used a low power $CO_2$ laser (25 W, Gaussian, continuous) for cutting 8 mm thick PMMA plates. A three-parameter, five-level full factorial experimental design has been applied to investigate the impact of the power (13-23 W), speed (202-586 mm/s), and several passes (1-5) on kerf angle. They developed regression predictive models for controlling the process and concluded that a higher number of passes, lower speed and higher power resulted in a lower kerf angle.

Empirical or soft computing (neural networks or genetic algorithms) models based on experimental design methods were also developed in the literature [22]. The most characteristic ones are presented in the following paragraphs.

Polymeric materials (PMMA, PC and PP) were investigated when a continuous $CO_2$ laser cut by Choudhury and Shirley [23]. Laser power (200-400W), speed (3.3-6.6mm/sec) and pressure (2.5-3.5Bar) tested, and the kerf characteristics (HAZ depth, Ra, dimensional deviation) were investigated using a linear ANOVA analysis. All plates had 3mm thickness. The central composite experimental design applied to reduce the experiments. They measured average surface roughness for PMMA plates up to 9 μm with a standard deviation of 1.1 μm and HAZ depth between 130-210 μm. They extracted predictive models based on the response surface methodology (RSM). It was concluded that the HAZ depth for all polymers increases with the increase of the power or decrease of the beam velocity and that the surface roughness was most affected by the laser speed and the air pressure.

Nukman et al. [24] studied the kerf width during $CO_2$ laser cutting of Perspex glass thin plates (3-5 mm). Laser power (100-500 W), cutting speed (3.3-20 mm/s), stand-off distance (1-10 mm) and gas pressure (0.5-4.5 bar) were tested. A four-parameter three-level Taguchi design based on the L9 orthogonal array is used. Two models, an FFBP and an optimized GA-Taguchi NN, were developed for the kerf width predictions. They measured kerf widths between 0.5-1.5 mm and concluded that the developed FFBP-NN was not appropriate for accurate predictions. Consequently, they used a hybrid Neural Network-Genetic Algorithm (NN-GA) model to improve predictions. With the hybrid model, the error reduced to below 10%.

Hossain et al. [17] studied the stand-off distance (1-10 mm), gas pressure (0.5-4.5 bar), velocity of cut (3.3-20 mm/s) and laser power (100-500 W), according to the minimum kerf width. The focal length was kept constant at 127 mm. They developed an intelligent fuzzy expert system (FES) model to predict the kerf width in $CO_2$ laser cutting of (3 mm) PMMA thin plates. The FES model was completed by eighty-one (81) experiments based on a four-parameter three-level full factorial design. They measured kerf widths between 0.5 and 1.5 mm and concluded that the predictions made by the FES model were satisfactory in terms of relative error and goodness of fit and that can be used in PMMA laser machining simulation.

Moradi et al. [10] studied the laser power (20-40 W), the cutting speed (2-18 mm/s) and the focal plane position (0 - 4 mm) during PMMA $CO_2$ laser cutting (3.2 mm). They used a central composite design (three-parameter five-level, 17 experiments), quadratic polynomial functions, and response surface methodology (RSM) to model the kerf characteristics; top and bottom kerf, kerfs ratio, HAZ and average surface roughness (Ra). They measured the HAZ depths between 0.15 to 0.45 mm, kerf widths (top and bottom) between 0.15 to 0.6 mm, and Ra between 1-15 μm. They found that increasing the cutting speed, reducing the focal position level, or reducing the laser power resulted in the reduced bottom kerf. They also concluded that when the focal plane was lower than the upper part surface, the kerf characteristics improved.

Moradi et al. [25] developed a finite element model to simulate the $CO_2$ laser cutting of (3.2 mm) PMMA plates. They concluded that increasing the laser cutting speed from 4 to 20 mm/s and decreasing the laser power from 50 to 20 W results in reducing the heat-affected zone. Also, it is mentioned that the depth of the kerf for different laser power values, speed and laser focal plane can be predicted by applying the proposed FEM model.

The effects of power (120-150 W), velocity (1.66-5 mm/s), gas pressure (1-3 bar) and plate thickness (4-12 mm) on the upper and down kerf width as well as on kerf angle have been experimentally investigated by Elsheikh et al. [26]. A continuous $CO_2$ laser was used (wavelength, 10.64 μm; constant stand-off distance, 6 mm; focal length, 50mm). An L18 Taguchi table (one parameter with two levels and three parameters with three-level) is implemented, and the kerf characteristics were statistically analysed using the ANOVA analysis. The kerf widths (top and bottom) were measured between 0.2 and 0.9mm, and the kerf angles between 0.01 to 2 degrees. They determined that the most dominant parameter was the thickness of the sheet, and when it increases, all the measurements of the 'kerf' decrease. The second most influential parameter was the cutting speed and found that when it increases, the kerf widths decrease. Finally, they developed regression models and applied a genetic algorithm to optimize the process.

Concluding, all the above investigations studied theoretically or experimentally the kerf characteristics of the thermoplastic PMMA thin plates (3-12 mm) within the following laser power and velocity ranges: (i) miniaturised structures: power bellow 2.5W and velocity up to 64 mm/s [20], or power between 13-23 W and velocities between 202-586 mm/s [18]; (ii) Thin plate cutting with power higher than 100 W and velocities up to 150 mm/s [21,1,19,23,24,17,26], or power between 20-40 W and velocities between 2-18 mm/s [10,25]. The kerf characteristics that measured were: (i) average surface roughness between 1-15 μm, (ii) kerf widths (top and bottom) between 0.1 to 1.5 mm, (iii) kerf angle between 0-2 degrees, and (iv) HAZ depth between 0.1-0.33 mm.

The above literature review demonstrates that there is a gap of experimental work for laser power between 50-100 W. The velocity and stand-off distance at the upper surface should be considered, too, when studying the kerf characteristics, as they are predominant parameters [10]. For 4 mm PMMA sheets and using about 90 W laser power, the upper limit for laser speed is about 30 mm/s in order to have laser penetration [27].

Thus, after preliminary work to have a thorough cut for all experiments was decided to include as tested parameters: the laser power (LP: 82.5-97.5 W), cutting speed (CS: 8-18 mm/s), and stand-off distance (SoD: 7-9 mm). A low-cost continuous wave $CO_2$ laser is utilized with a max power of 150 W. The thickness of

the PMMA plates selected to be 4 mm as proposed by the literature review. A three-parameter three-level ($3^3$) full factorial experimental design is selected for investigating the proposed kerf characteristics experimentally (Wu, Wm, Wd and KA) [28,29]. The effects of process parameters and their interactions are analysed using statistical analysis tools, and NN modeling is proposed due to strong parameter interactions. The methodology proposed in [30,31] regarding the implementation of statistical methods for the post-processing of experimental data guides the present work.

## 2. Materials And Methods

A low power continuous $CO_2$ laser ( BODOR model BCL 1325B; wavelength 10.6 μm) was used for conducting the experiments [32]. A conical convergent nozzle with a tip diameter of 2 mm is utilised. The configuration of the mirrors and lens is shown in Fig. 1a. The assist gas was air at 1 bar constant pressure. Beam focal length adjusted at 46 mm when the stand-off distance (SoD) is 8 mm from the upper surface. In this SoD, the laser spot diameter is about 0.3 mm. The airflow distribution and the spot diameter at the upper surface change when the SoD changes. The experimental cuts were designed using the Laser Engraving & Cutting Software RDWorks8.0 [33].

The laser nozzle tip is set in a different stand-off distance for each of the three PMMA work-pieces, at 7, 8 and 9 mm, respectively. The cuts were straight lines with a length of 10 mm in the X direction (Fig. 2b). All the workpieces were of a 4 mm thickness PMMA with a melting point of 160$^o$C and a density of 1.18 g/cm$^3$.

The upper (Wu), middle (Wm) and down (Wd) kerf width were measured using an optical microscope [34], and readings were obtained with the 'ImageJ' software [33]; see Fig. 2c. The upper and down kerf widths were measured as an average of four measurements (T1-T4; B1-B4), while middle kerf width readings as an average of three values (F1-F3), Fig. 2d. The kerf angle (KA) was calculated using the following formula (Eq. 1; [26]):

$$KA(\deg)=\tan^{-1}\left(\frac{Wu-Wd}{2*4}\right) \quad (1)$$

where 4 is the specimens thickness in mm.

## 2.1. Design of experiments

A three-parameter three-level full factorial experimental design is used ($3^3$) (Table 1). This experimental design is utilised in contrast with the literature that the fractional factorial (Taguchi, CCD, or mixed) design is used [24,26,10,17,23] to obtain more experiments for the statistical modelling process [35]. Twenty-seven measurements of kerf widths and kerf angles are tabulated in Table 2. The Stand-off Distance (SoD, mm), Cutting Speed (CS, mm/s), and Laser Power (LP, W) are used as input parameters (columns 2-4), while the last four columns are used for the upper (Wu, mm), middle (Wm, mm), down (Wd, mm) kerf widths and Kerf Angle (KA, deg).

For selecting the parameter, factor, levels, the following procedure was followed. Initially, the laser power levels were selected (82.5, 90 and 97.5W). These values have not been tested before in literature for kerf optimization. Prior to this, preliminary cuts were undertaken in order to select the beam velocity levels. It was found that the 8, 13, and 18 mm/s cutting speed values cut all nine combinations with the following power values: 82.5, 90 and 97.5W at a stand-off distance of 8 mm. These values are following those proposed in [27]. Then, the average surface roughness is measured, resulting in similar range values (lower than 5 μm) than those stated in the literature [21,23,36]. Having undertaken a number of different setups (with regard to the stand-off distance) maintaining the same aforementioned parameters, all PMMA's cuts were executed completely at the 7 and 9 mm stand-off distances. Finally, the gas pressure was not investigated and kept constant at 1 bar because Ra values close to 0.61 μm were achieved (see [36]), very close to mechanical cutting processes.

Additionally, in order to investigate how the stand-off distance (SoD) affects the upper and down kerf widths with values smaller than 7 mm (Fig. 3a), six cuts performed with SoD of 6, 5, 4, 3, 2 and 1 mm, respectively. It was concluded if the stand-off distance is smaller than 7mm, the resulting kerf is not acceptable (Wu bigger than 0.8 mm; Fig. 3b).

**Table 1** The three-parameter three-level ($3^3$) design

| No | Process Parameter | Level 1 | Level 2 | Level 3 |
|---|---|---|---|---|
| 1 | Stand-off distance-SoD (mm) | 7 | 8 | 9 |
| 2 | Cutting Speed-CS (mm/s) | 8 | 13 | 18 |
| 3 | Laser Power-LP (W) | 82.5 | 90 | 97.5 |

**Table 2** Full experimental array for the kerf widths and kerf angle

| | Input parameters | | | Output parameters | | | |
|---|---|---|---|---|---|---|---|
| No | SoD (mm) | CS (mm/s) | LP (W) | Wu (mm) | Wm (mm) | Wd (mm) | KA(deg) |
| 1 | 7 | 8 | 82.5 | 0.438 | 0.443 | 0.453 | -0.11 |
| 2 | 7 | 8 | 90.0 | 0.424 | 0.421 | 0.406 | 0.13 |
| 3 | 7 | 8 | 97.5 | 0.427 | 0.436 | 0.405 | 0.16 |
| 4 | 7 | 13 | 82.5 | 0.337 | 0.320 | 0.307 | 0.21 |
| 5 | 7 | 13 | 90.0 | 0.343 | 0.320 | 0.294 | 0.35 |
| 6 | 7 | 13 | 97.5 | 0.336 | 0.343 | 0.318 | 0.13 |
| 7 | 7 | 18 | 82.5 | 0.326 | 0.274 | 0.224 | 0.73 |
| 8 | 7 | 18 | 90.0 | 0.372 | 0.312 | 0.232 | 1.00 |
| 9 | 7 | 18 | 97.5 | 0.366 | 0.325 | 0.272 | 0.67 |
| 10 | 8 | 8 | 82.5 | 0.478 | 0.477 | 0.446 | 0.23 |
| 11 | 8 | 8 | 90.0 | 0.477 | 0.469 | 0.434 | 0.31 |
| 12 | 8 | 8 | 97.5 | 0.470 | 0.457 | 0.430 | 0.29 |
| 13 | 8 | 13 | 82.5 | 0.445 | 0.395 | 0.345 | 0.71 |
| 14 | 8 | 13 | 90.0 | 0.431 | 0.388 | 0.337 | 0.68 |
| 15 | 8 | 13 | 97.5 | 0.428 | 0.376 | 0.326 | 0.73 |
| 16 | 8 | 18 | 82.5 | 0.429 | 0.358 | 0.298 | 0.93 |
| 17 | 8 | 18 | 90.0 | 0.422 | 0.350 | 0.294 | 0.91 |
| 18 | 8 | 18 | 97.5 | 0.401 | 0.366 | 0.289 | 0.80 |
| 19 | 9 | 8 | 82.5 | 0.575 | 0.479 | 0.539 | 0.69 |
| 20 | 9 | 8 | 90.0 | 0.507 | 0.414 | 0.480 | 0.67 |
| 21 | 9 | 8 | 97.5 | 0.516 | 0.458 | 0.501 | 0.42 |
| 22 | 9 | 13 | 82.5 | 0.484 | 0.298 | 0.405 | 1.33 |
| 23 | 9 | 13 | 90.0 | 0.476 | 0.286 | 0.390 | 1.36 |
| 24 | 9 | 13 | 97.5 | 0.428 | 0.251 | 0.361 | 1.27 |
| 25 | 9 | 18 | 82.5 | 0.435 | 0.174 | 0.325 | 1.87 |
| 26 | 9 | 18 | 90.0 | 0.422 | 0.163 | 0.326 | 1.85 |
| 27 | 9 | 18 | 97.5 | 0.434 | 0.192 | 0.330 | 1.73 |
| Average | | | | 0.431 | 0.388 | 0.327 | 0.74 |
| St.dev. | | | | 0.059 | 0.068 | 0.091 | 0.54 |
| Min | | | | 0.326 | 0.274 | 0.163 | -0.11 |
| Max | | | | 0.575 | 0.539 | 0.479 | 1.87 |

## 3. Experimental Results And Analysis

The experimental results initially were analysed using main effect plots (Fig. 4). These plots, also known as ANOM diagrams for averages of level sets, are descriptive and can demonstrate which parameter mostly affects the quality measurement.

According to these plots, cutting speed (CS) mean values have the biggest variance for upper, middle and down kerf width and the kerf angle metrics. The increase of cutting speed redistributes the energy inside the kerf geometry resulting in smaller upper widths, even smaller down widths and higher kerf angles.

The stand-off distance (SoD) is very critical for the upper kerf width and the kerf angle. The decrease of SoD from 9 to 8 mm, decreases the spot diameter at the upper surface and redistribute the airflow on the upper surface resulting in better upper kerf width and kerf angle (See Fig. 3a). Then when SoD becomes 7 mm, all the kerf attributes improved, resulting in widths closer to 0.3 to 0.4 mm and kerf angles closer to 0.4 degrees.

Finally, the laser power (LP) changes are not critical for all the kerf attributes at the specific experimental area studied. The higher value of 97.5 W optimises the upper kerf width and kerf angle. The redistribution of energy and mass flow that causes are not capable of greater changes in kerf attributes.

The parameters' level that results in the best kerf metrics is calculated as well. Using a cutting speed of 18 mm/s minimises the kerf widths (Wu, Wm and Wd) and maximises the kerf angle (KA). On the other hand, a stand-off distance of 7 mm minimises the upper kerf width, whereas the stand-off distance that minimises the down kerf width is 9 mm. The kerf angle is optimised when the cutting speed is 8 mm/s and the stand-off distance 7 mm. The laser power mean values are shown small variances, and hence they did not take into account.

Then the ANOVA analysis (Table 3-6) is applied. Following that, the interactions between the stand-off distance and the cutting speed are investigated. At the same time, according to the ANOVA analysis, these two parameters have a significant impact on all kerf metrics ($F>4$, $P<0.05$). Additionally, the laser power was insignificant in the proposed experimental area for all kerf metrics ($F<2$ and $P>0.05$) [35]. The main effect plots also show that the stand-off distance and the cutting speed result in major spreads while laser power is not.

The 7 mm stand-off distance optimises the Wu, Wm and KA while the 9 mm optimises the Wd. The 18 mm/s cutting speed optimises the Wu, Wm and Wd and the 8mm/s the KA. The laser power is proven to have an insignificant impact on the kerf metrics. Optimised values for each of the kerf metrics can be concluded straightforwardly by the main effect plots (ANOM analysis, Fig. 4).

The ANOVA analysis demonstrated that the key parameter affecting the upper kerf width and kerf angle is the stand-off distance (52% and 48%, respectively). In comparison, the cutting speed dominates for the middle and down widths (79% and 84%, respectively). The error percentage of ANOVA linear analysis is about 15 % for all metrics concerning the Rsq predicting values.

**Table 3** ANOVA for the upper kerf width (Wu)

| | DoF | SoS | MS | F | P | % |
|---|---|---|---|---|---|---|
| SoD | 2 | 0.047755 | 0.023877 | 52.13 | 0.000 | 52.8 |
| CS | 2 | 0.032477 | 0.016239 | 35.45 | 0.000 | 35.9 |
| LP | 2 | 0.001077 | 0.000539 | 1.18 | 0.329 | 1.2 |
| Error | 20 | 0.009160 | 0.000458 | | | 10.1 |
| Total | 26 | 0.090470 | | | | |
| R-sq | | | | | | 89.9 |
| R-sq(adj) | | | | | | 86.8 |
| R-sq(pred) | | | | | | 81.5 |

**Table 4** ANOVA for middle kerf width (Wm)

| | DoF | SoS | MS | F | P | % |
|---|---|---|---|---|---|---|
| SoD | 2 | 0.015236 | 0.007618 | 16.89 | 0.000 | 12.8 |
| CS | 2 | 0.094141 | 0.047070 | 104.36 | 0.000 | 79.3 |
| LP | 2 | 0.000356 | 0.000178 | 0.39 | 0.679 | 0.3 |
| Error | 20 | 0.009021 | 0.000451 | | | 7.6 |
| Total | 26 | 0,118754 | | | | 12.8 |
| R-sq | | | | | | 92.4 |
| R-sq(adj) | | | | | | 90.1 |
| R-sq(pred) | | | | | | 86.1 |

**Table 5** ANOVA for down kerf width (Wd)

| | DoF | SoS | MS | F | P | % |
|---|---|---|---|---|---|---|
| SoD | 2 | 0.013247 | 0.006623 | 6.76 | 0.006 | 6.1 |
| CS | 2 | 0.182492 | 0.091246 | 93.19 | 0.000 | 84.2 |
| LP | 2 | 0.001472 | 0.000736 | 0.75 | 0.484 | 0.7 |
| Error | 20 | 0.019583 | 0.000979 | | | 9.0 |
| Total | 26 | 0.216794 | | | | |
| R-sq | | | | | | 90.9 |
| R-sq(adj) | | | | | | 88.2 |
| R-sq(pred) | | | | | | 83.5 |

**Table 6** ANOVA for down kerf angle (KA)

| | DoF | SoS | MS | F | P | % |
|---|---|---|---|---|---|---|
| SoD | 2 | 3.68185 | 1.84093 | 61.47 | 0.000 | 48.1 |
| CS | 2 | 3.31540 | 1.65770 | 55.35 | 0.000 | 43.3 |
| LP | 2 | 0.06320 | 0.03160 | 1.06 | 0.367 | 0.8 |
| Error | 20 | 0.59901 | 0.02995 | | | 7.8 |
| Total | 26 | 7.65947 | | | | |
| R-sq | | | | | | 92.1 |
| R-sq(adj) | | | | | | 89.8 |
| R-sq(pred) | | | | | | 85.7 |

The interactions charts between the stand-off distance and the cutting speed follow as these two parameters are the most important ones (see the ANOVA analysis). These interactions charts (Fig. 5) show an antisynergistic relation between the stand-off distance and the cutting speed. For such interactions, non-linear or neural network models have been used to achieve accurate predictions [37]. Finally, in Fig. 6, the surfaces plots for all metrics illustrated according to the cutting speed and the stand-off distance.

## 3.1 FFBP-NN set up

After the ANOVA analysis and interactions study, four separately FeedForward BackPropagation Neural Network (FFBP-NN) models were developed to predict the kerf geometry (upper, middle and down widths and kerf angle) [38]. Upper, middle and down kerf widths (Wu, Wm and Wd), and kerf angle (KA) are used as output vectors for the four apart FFBP-NNs, while the Stand-off Distance, Cutting Speed, Laser Power and the constant value one (SoD, CS, LP and 1) as input parameters (see Fig. 7a). All input and output are normalized in the range of 0 to 1, using the map min-max method. Normalization is suggested for better training performance and generalization capability [39]. The data randomly separated into three sub-datasets: training (70 %), validation (15 %) and test (15 %).

The “nntool” toolbox (MATLAB R2015) has been used to develop the FFBP-NN model. For similar mechanical applications, where the performance metrics have to be assigned according to the input parameters, a simple FFBP-NN with one hidden layer is considered adequate [40].

The typical BackPropagation (BP) algorithm is used for the NN training procedure. BackPropagation is a Gradient Descent (GD) algorithm that minimises the Mean Square Error (MSE). Levenberg-Marquardt algorithm (trainlm) is used as a training function to solve non-linear least squares curve fitting [41]. The adaptation learning function is the ‘learngdm’, which updates the weight and bias values according to Levenberg-Marquardt optimization [42,43]. The initial momentum parameter ‘mu’ has been set at 0.3, the ‘mu’ decrease factor at 0.1, while the ‘mu’ increase factor at 10 and the ‘mu’ maximum at $10^{\wedge 10}$. The

training process stops when the maximum number of epochs equals 1000. The performance is minimized to zero, or the performance gradient falls below $10^{\wedge(-7)}$ and finally when the maximum validation failures become six (6).

For the hidden layer, eight neurons have been used (Fig. 7a), alongside the hyperbolic tangent sigmoid (tansig) transfer function (Fig. 7b), while linear function (purelin) has been used for the output (Fig. 7c). The number of neurons in the hidden layer is decided after simulations between six, eight, and twelve. All four FFBP-NN models have the same topology and learning parameters.

By implementing this topology and after three repetitions, we get R values that exceed 0.98 for all the different datasets (training, validation, test and all), as depicted in Figures 8-11 for the kerf attributes.

All predictions are very close to actual values (Table 7, Fig. 12b). For the given datasets and topology, the MSE of kerf angle (KA) optimised at 0.0014647, epoch 0 (Figure 12a). By studying the residuals plots of the KA, the errors are distributed without significant deviations between the datasets, increasing the significance of the R correlation coefficient as a performance metric of this NN model (Fig. 12c). The same conclusions are observed for all kerf attributes. To this end, the full factorial experimental work offers enough data to train the model to predict the desired, process-related outputs with high accuracy.

**Table 7** FFBP-NN errors

| | Actual | | | | Predected | | | |
|---|---|---|---|---|---|---|---|---|
| No | Wu-a | Wm-a | Wd-a | KA-a | Wu-p | Wm-p | Wd-p | KA-p |
| 1 | 0.438 | 0.443 | 0.453 | -0.11 | 0.464 | 0.423 | 0.432 | -0.010 |
| 2 | 0.425 | 0.421 | 0.407 | 0.13 | 0.437 | 0.447 | 0.408 | 0.090 |
| 3 | 0.427 | 0.436 | 0.405 | 0.16 | 0.428 | 0.417 | 0.411 | 0.018 |
| 4 | 0.337 | 0.320 | 0.307 | 0.21 | 0.332 | 0.325 | 0.319 | 0.247 |
| 5 | 0.343 | 0.320 | 0.295 | 0.35 | 0.344 | 0.330 | 0.310 | 0.287 |
| 6 | 0.336 | 0.343 | 0.318 | 0.13 | 0.341 | 0.339 | 0.310 | 0.191 |
| 7 | 0.326 | 0.274 | 0.224 | 0.73 | 0.341 | 0.300 | 0.226 | 0.696 |
| 8 | 0.372 | 0.312 | 0.232 | 1.00 | 0.358 | 0.312 | 0.225 | 0.674 |
| 9 | 0.366 | 0.325 | 0.272 | 0.67 | 0.371 | 0.329 | 0.276 | 0.656 |
| 10 | 0.478 | 0.477 | 0.446 | 0.23 | 0.510 | 0.485 | 0.462 | 0.257 |
| 11 | 0.477 | 0.469 | 0.434 | 0.31 | 0.477 | 0.485 | 0.433 | 0.342 |
| 12 | 0.471 | 0.457 | 0.430 | 0.29 | 0.468 | 0.468 | 0.431 | 0.375 |
| 13 | 0.445 | 0.395 | 0.345 | 0.71 | 0.447 | 0.381 | 0.330 | 0.679 |
| 14 | 0.432 | 0.388 | 0.337 | 0.68 | 0.435 | 0.385 | 0.336 | 0.708 |
| 15 | 0.428 | 0.376 | 0.326 | 0.73 | 0.420 | 0.376 | 0.324 | 0.776 |
| 16 | 0.429 | 0.358 | 0.298 | 0.93 | 0.428 | 0.335 | 0.291 | 0.954 |
| 17 | 0.422 | 0.350 | 0.294 | 0.91 | 0.424 | 0.352 | 0.289 | 0.885 |
| 18 | 0.401 | 0.366 | 0.289 | 0.80 | 0.406 | 0.363 | 0.289 | 0.855 |
| 19 | 0.575 | 0.539 | 0.479 | 0.69 | 0.551 | 0.524 | 0.463 | 0.568 |
| 20 | 0.508 | 0.480 | 0.414 | 0.67 | 0.507 | 0.465 | 0.437 | 0.592 |
| 21 | 0.516 | 0.501 | 0.458 | 0.42 | 0.499 | 0.492 | 0.433 | 0.538 |
| 22 | 0.484 | 0.405 | 0.298 | 1.33 | 0.490 | 0.410 | 0.300 | 1.323 |
| 23 | 0.476 | 0.390 | 0.286 | 1.36 | 0.465 | 0.382 | 0.292 | 1.348 |
| 24 | 0.428 | 0.361 | 0.251 | 1.27 | 0.436 | 0.385 | 0.237 | 1.304 |
| 25 | 0.435 | 0.325 | 0.174 | 1.87 | 0.432 | 0.324 | 0.175 | 1.852 |
| 26 | 0.422 | 0.326 | 0.163 | 1.85 | 0.427 | 0.340 | 0.158 | 1.836 |
| 27 | 0.434 | 0.330 | 0.192 | 1.73 | 0.424 | 0.335 | 0.192 | 1.783 |

## 4. Conclusions

An FFBP-NN has been implemented in this work to predict the kerf geometry of (4mm) PMMA thin plates during the continuous low power $CO_2$ laser cutting process. Stand-off distance (7, 8 and 9 mm), cutting speed (8, 13 and 18 mm/s), and laser power (82.5, 90 and 97.5 W) were used as input and kerf geometry attributes (upper, middle and down kerf widths, and kerf angle) as output parameters, respectively.

A full factorial experimental design ($L_{27}$: $3^3$ design) is used, and statistical modelling is followed. The experimental and statistical study showed that:

- the dominant parameter is stand-off distance for the upper kerf width and kerf angle,
- the cutting speed is the most significant parameter for the middle and down kerf widths,
- strong interactions recorded between the cutting speed and stand-off distance, and
- the parameter values which optimize the kerf angle resulting in positive values close to zero degrees, were the 7 mm stand-off distance, 8 mm/s cutting speed and 97.5 W laser power.

After that, a Feed-Forward Back Propagation Neural Network (FFBP-NN) trained, validated and generalised, having one hidden layer and eight neurons as proposed by similar studies in the literature. All data normalized using the map min-max rule. Using the proposed 'FFBP-NN' models, the upper, middle and lower kerf width, and the kerf angle optimised for better production times and smaller kerf angles. All average surface measurements (Ra) for the 8 mm stand-off distance are lower than 5 μm, following the literature [21,23,36].

As future work, the authors propose applying neural networks for predicting more kerf characteristics like the average surface roughness and the HAZ zone depth. Also, the investigation of assist gas pressure and the expanse of laser power range and PMMA thickness is suggested.

## Declarations

The authors declare that they have no conflict of interest.

Funding Source

This research did not receive any specific grant from funding agencies in the public, commercial, or not-for-profit sectors.

Author Contributions:

Conceptualization, J.K. and K.N.; methodology, J.K. and K.N; software, J.K., P.S and K.S; validation, J.K. and P.S.; formal analysis K.N.; investigation, K.N.; resources, J.K.; writing—original draft preparation, J.K., K.N. P.S. and K.S.; review and editing, J.K., K.N, P.S. and K.S.; suppererversion, J.K.; project administration, J.K.; All authors have read and agreed to the published version of the manuscript.

Data Availability Statements

The datasets generated during and/or analysed during the current study are available in the [Research Square] repository, [https://www.researchsquare.com/article/rs-268745/v1].

## References

1. Davim JP, Barricas N, Conceicao M, Oliveira C (2008) Some experimental studies on CO2 laser cutting quality of polymeric materials. Journal of materials processing technology 198 (1-3):99-104

2. Mushtaq RT, Wang Y, Rehman M, Khan AM, Mia M (2020) State-Of-The-Art and Trends in CO2 Laser Cutting of Polymeric Materials—A Review. Materials 13 (17):3839

3. Romoli L, Tantussi G, Dini G (2011) Experimental approach to the laser machining of PMMA substrates for the fabrication of microfluidic devices. Optics and Lasers in Engineering 49 (3):419-427

4. Muangpool T, Pullteap S Reviews on laser cutting technology for industrial applications. In: Third International Conference on Photonics Solutions (ICPS2017), 2018. International Society for Optics and Photonics, p 107140Q

5. Haddadi E, Moradi M, Karimzad Ghavidel A, Karimzad Ghavidel A, Meiabadi S (2019) Experimental and parametric evaluation of cut quality characteristics in CO2 laser cutting of polystyrene. Optik 184:103-114. doi:https://doi.org/10.1016/j.ijleo.2019.03.040

6. Moradi M, Abdollahi H (2017) Statistical modelling and optimization of the laser percussion microdrilling of thin sheet stainless steel. Journal of lasers in Engineering

7. Chryssolouris G (2013) Laser machining: theory and practice. Springer Science & Business Media,

8. Stournaras A, Stavropoulos P, Salonitis K, Chryssolouris G (2009) An investigation of quality in CO2 laser cutting of aluminum. CIRP Journal of Manufacturing Science and Technology 2 (1):61-69

9. Zhou BH, Mahdavian S (2004) Experimental and theoretical analyses of cutting nonmetallic materials by low power CO2-laser. Journal of materials processing technology 146 (2):188-192

10. Moradi M, Mehrabi O, Azdast T, Benyounis KY (2017) Enhancement of low power CO2 laser cutting process for injection molded polycarbonate. Optics & Laser Technology 96:208-218

11. Tamrin K, Nukman Y, Choudhury I, Shirley S (2015) Multiple-objective optimization in precision laser cutting of different thermoplastics. Optics and Lasers in Engineering 67:57-65

12. Cardoso RM, Santos ROd, Munoz RA, Garcia CD, Blanes L (2020) A Multi-Pump Magnetohydrodynamics Lab-On-A-Chip Device for Automated Flow Control and Analyte Delivery. Sensors 20 (17):4909

13. Conzelmann J, Schwarz FB, Hamm B, Scheel M, Jahnke P (2020) Development of a method to create uniform phantoms for task-based assessment of CT image quality. Journal of Applied Clinical Medical Physics 21 (9):201-208

14. Sen A, Doloi B, Bhattacharyya B (2020) Parametric influences of fiber laser micro-machining for the generation of micro-channels on PMMA. Journal of the Brazilian Society of Mechanical Sciences and Engineering 42 (8):1-13

15. Lubis L, Hariyati I, Ryangga D, Mu'minah I, Mart T, Soejoko D (2020) Construction and Evaluation of a Multipurpose Performance Check Phantom for Computed Tomography. Atom Indonesia 46 (2):69-75

16. Çaydaş U, Hasçalık A (2008) Use of the grey relational analysis to determine optimum laser cutting parameters with multi-performance characteristics. Optics & laser technology 40 (7):987-994

17. Hossain A, Hossain A, Nukman Y, Hassan M, Harizam M, Sifullah A, Parandoush P (2016) A fuzzy logic-based prediction model for kerf width in laser beam machining. Materials and Manufacturing Processes 31 (5):679-684

18. Varsi AM, Shaikh AH (2019) Experimental and statistical study on kerf taper angle during CO2 laser cutting of thermoplastic material. Journal of Laser Applications 31 (3):032010

19. Davim JP, Oliveira C, Barricas N, Conceição M (2008) Evaluation of cutting quality of PMMA using CO 2 lasers. The International Journal of Advanced Manufacturing Technology 35 (9-10):875-879

20. Nayak NC, Lam Y, Yue C, Sinha AT (2008) CO2-laser micromachining of PMMA: the effect of polymer molecular weight. Journal of micromechanics and microengineering 18 (9):095020

21. Caiazzo F, Curcio F, Daurelio G, Minutolo FMC (2005) Laser cutting of different polymeric plastics (PE, PP and PC) by a CO2 laser beam. Journal of Materials Processing Technology 159 (3):279-285

22. Karagiannis S, Stavropoulos P, Ziogas C, Kechagias J (2014) Prediction of surface roughness magnitude in computer numerical controlled end milling processes using neural networks, by considering a set of influence parameters: an aluminium alloy 5083 case study. Proceedings of the Institution of Mechanical Engineers, Part B: Journal of Engineering Manufacture 228 (2):233-244

23. Choudhury IA, Shirley S (2010) Laser cutting of polymeric materials: an experimental investigation. Optics & Laser Technology 42 (3):503-508

24. Nukman Y, Hassan M, Harizam M (2013) Optimization of prediction error in CO2 laser cutting process by Taguchi artificial neural network hybrid with genetic algorithm. Applied Mathematics & Information Sciences 7 (1):363-370

25. Moradi M, Moghadam MK, Shamsborhan M, Beiranvand ZM, Rasouli A, Vahdati M, Bakhtiari A, Bodaghi M (2020) Simulation, statistical modeling, and optimization of CO2 laser cutting process of polycarbonate sheets. Optik:164932

26. Elsheikh AH, Deng W, Showaib EA (2020) Improving laser cutting quality of polymethylmethacrylate sheet: experimental investigation and optimization. Journal of Materials Research and Technology 9 (2):1325-1339

27. Atanasov P, Baeva M (1997) CW CO2 laser cutting of plastics, vol 3092. XI International Symposium on Gas Flow and Chemical Lasers and High Power Laser Conference. SPIE,

28. Karagiannis S, Ispoglou T, Stavropoulos P, Kechagias J Multi parameter optimization using Taguchi L8 (27) Array-A case study on additive paper lamination process. In: Proceedings of the 1st International Conference on Mathematical Methods & Computational Techniques in Science & Engineering, MMCTSE 2014, Athens, Gr, 2014. pp 110-113

29. Kechagias JD, Ninikas K, Petousis M, Vidakis N, Vaxevanidis N (2021) An investigation of surface quality characteristics of 3D printed PLA plates cut by CO2 laser using experimental design. Materials and Manufacturing Processes:1-10. doi:10.1080/10426914.2021.1906892

30. Kechagias J, Stavropoulos P, Koutsomichalis A, Ntintakis I, Vaxevanidis N (2014) Dimensional accuracy optimization of prototypes produced by PolyJet direct 3D printing technology. Advances in Engineering Mechanics and Materials:61-65

31. Stavropoulos P, Salonitis K, Stournaras A, Pandremenos J, Paralikas J, Chryssolouris G Experimental investigation of micro-milling process quality. In: 40th CIRP International Seminar on Manufacturing Systems, Liverpool, 2007.

32. Anon (2020) bodor. www.bodor.com/en/. Accessed 18/09/2020

33. Anon (2020) rdworks. https://rdworks.software.informer.com/8.0/. Accessed 18/09/2020

34. Anon (2020) irishelectronics. https://irishelectronics.ie/WebRoot/Register365/Shops/950018241/5CBE/ED52/5AF1/8897/B735/C0A8/190E/F401/Digital_Microscope_General_Instruction Accessed 28/09/2020

35. Kechagias JD, Aslani K-E, Fountas NA, Vaxevanidis NM, Manolakos DE (2020) A comparative investigation of Taguchi and full factorial design for machinability prediction in turning of a titanium alloy. Measurement 151:107213

36. Ninikas K, Kechagias J, Salonitis K (2021) The Impact of Process Parameters on Surface Roughness and Dimensional Accuracy during CO2 Laser Cutting of PMMA Thin Sheets. Journal of Manufacturing and Materials Processing 5 (3):74

37. Phadke MS (1995) Quality engineering using robust design. Prentice Hall PTR,

38. Omidvar M, Fard RK, Sohrabpoor H, Teimouri R (2015) Selection of laser bending process parameters for maximal deformation angle through neural network and teaching–learning-based optimization algorithm. Soft Computing 19 (3):609-620

39. Kim KS, Choi HH, Moon CS, Mun CW (2011) Comparison of k-nearest neighbor, quadratic discriminant and linear discriminant analysis in classification of electromyogram signals based on the wrist-motion directions. Current applied physics 11 (3):740-745

40. Vidakis N, Petousis M, Vaxevanidis N, Kechagias J (2020) Surface Roughness Investigation of Poly-Jet 3D Printing. Mathematics 8 (10):1758

41. Kechagias J, Tsiolikas A, Asteris P, Vaxevanidis N Optimizing ANN performance using DOE: application on turning of a titanium alloy. In: MATEC Web of Conferences, 2018. EDP Sciences, p 01017

42. Kechagias J, Iakovakis V (2009) A neural network solution for LOM process performance. The International Journal of Advanced Manufacturing Technology 43 (11-12):1214-1222

43. Žic M, Subotić V, Pereverzyev S, Fajfar I (2020) Solving CNLS problems using Levenberg-Marquardt algorithm: A new fitting strategy combining limits and a symbolic Jacobian matrix. Journal of Electroanalytical Chemistry 866:114171

## Figures

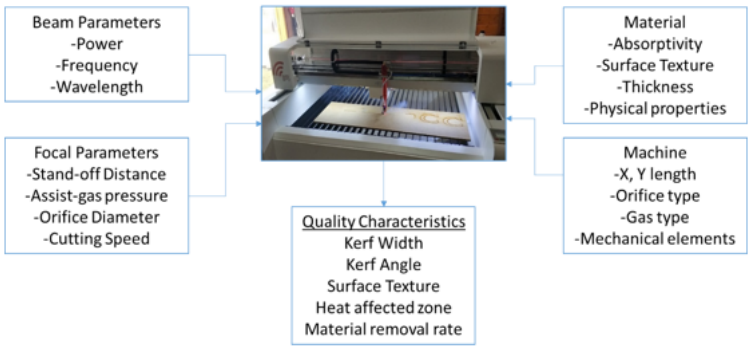


**Figure 1**

Process parameter and quality characteristics of laser cutting.

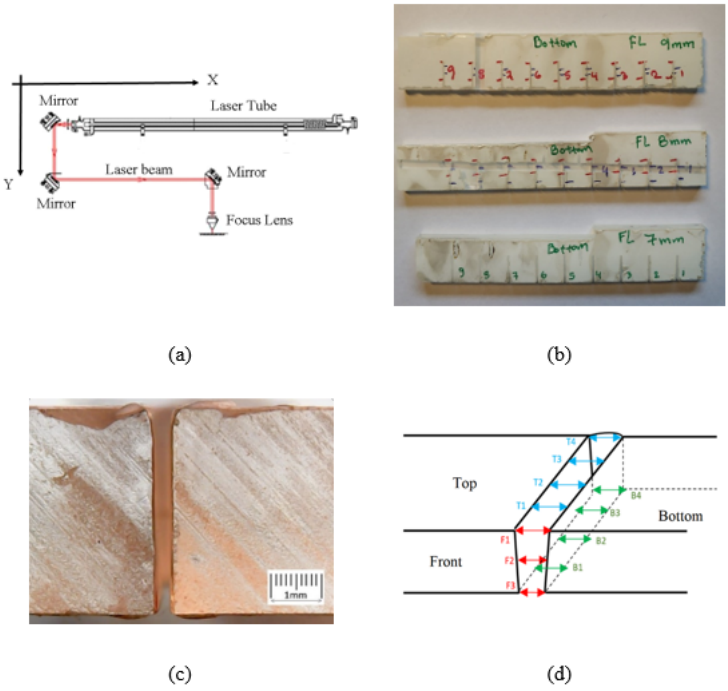

Figure 2

(a) Mirrors and lence configuration, (b) Cut work-pieces, (c) microscope image, and (d) kerf width measurements

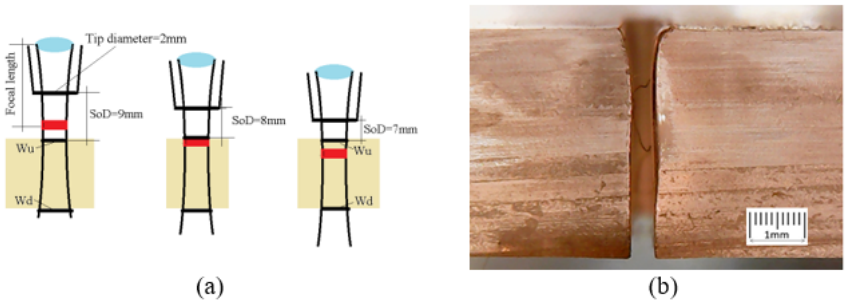


Figure 3

(a) Effects of SoD on kerf width and (b) Kerf widths (Wu=0.816 mm, Wd=0.393 mm) when SoD = 6 mm, LP = 82.5 W and CS = 8 mm/s

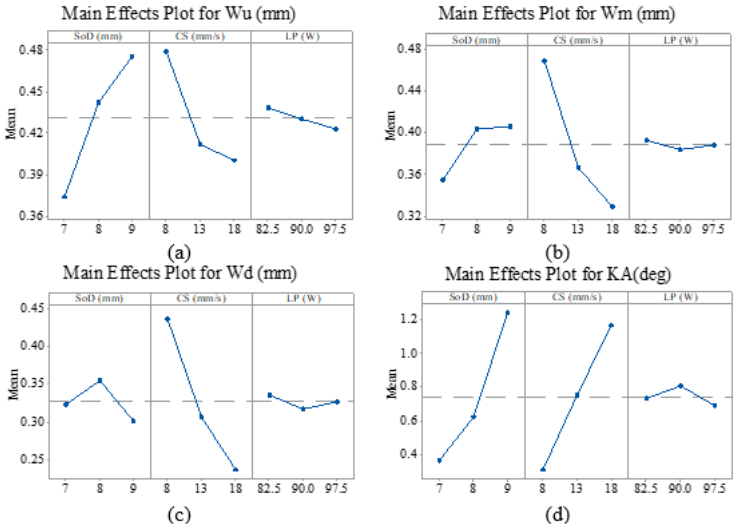


Figure 4

ANOM diagrams for kerf width metrics

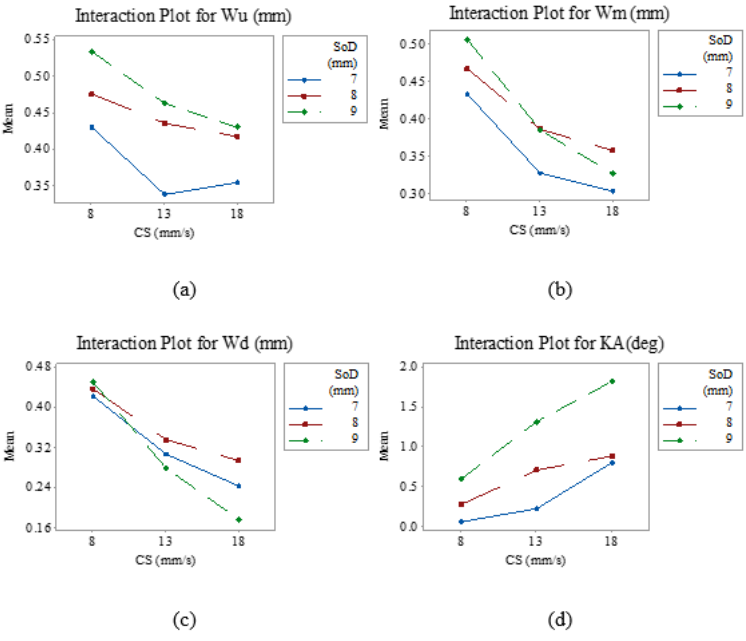


Figure 5

Interaction plots between stand-off distance and cutting speed

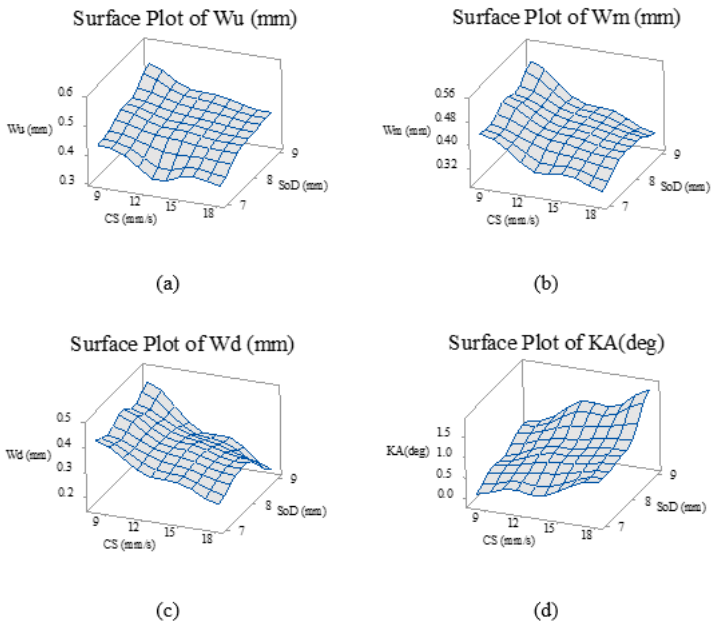


**Figure 6**

Surface plots for kerf widths and kerf angle

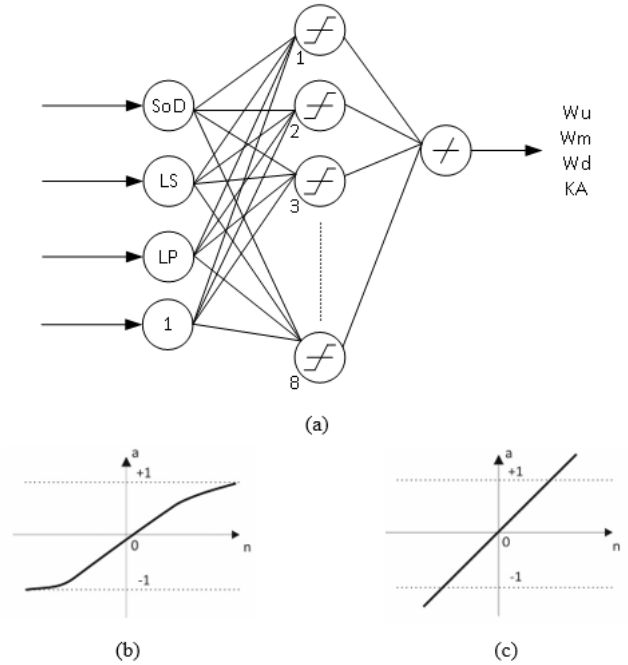


**Figure 7**

(a) FFBP-NN models topology, (b) Linear transfer function (purelin) and (c) Hyperbolic tangent sigmoid transfer function (tansig)

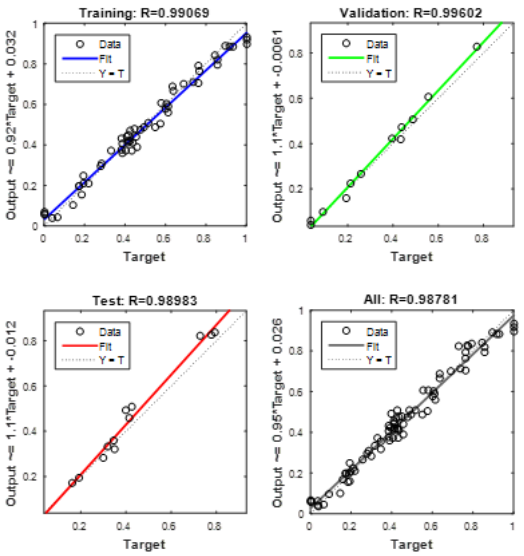


**Figure 8**

Training and performance of the FFBP-NN for Wu attribute.

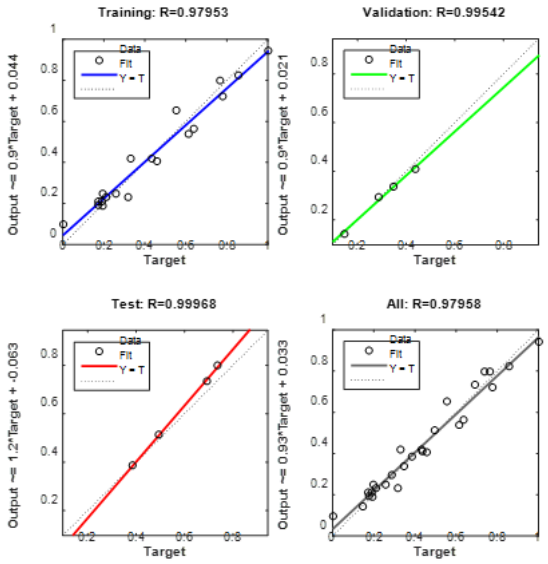


**Figure 9**

Training and performance of the FFBP-NN for Wm attribute.

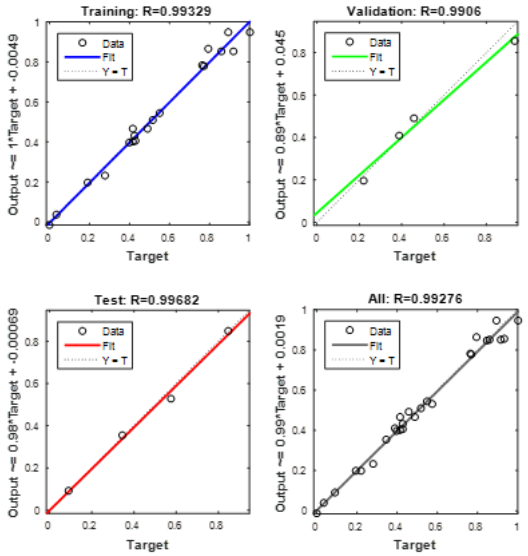


Figure 10

Training and performance of the FFBP-NN for Wd attribute.

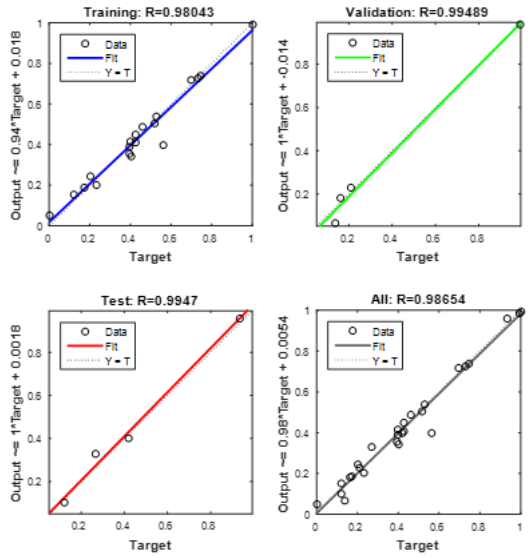


Figure 11

Training and performance of the FFBP-NN for KA attribute.

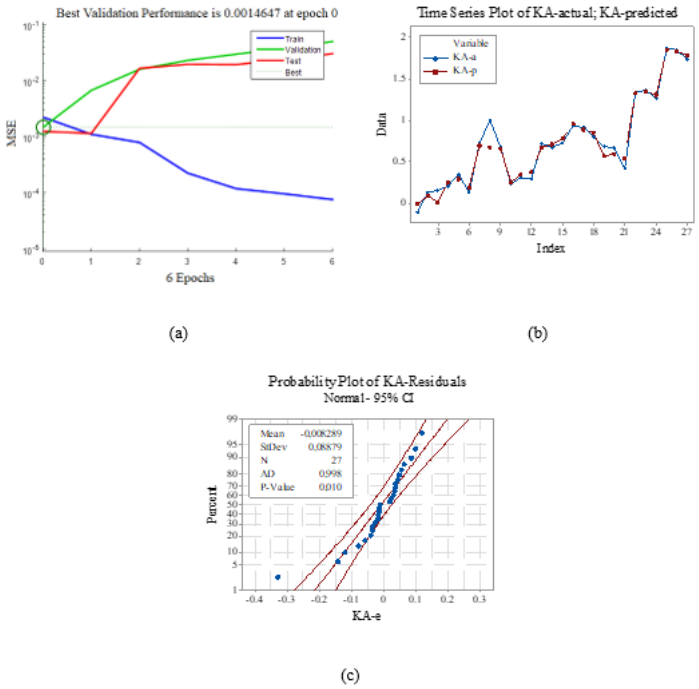


Figure 12

(a) Training of FFBP-NN for KA attribute, (b) Actual and predicted values for kerf angle (KA) and (c) residual plots for kerf angle (KA)